Nanoscale

PAPER

View Article Online
View Journal | View Issue

Cite this: *Nanoscale*, 2014, **6**, 1833

Dielectric response of pentagonal defects in multilayer graphene nano-cones

F. S. Hage,*[abc] D. M. Kepaptsoglou,[a] C. R. Seabourne,[d] Q. M. Ramasse,*[a] A. J. Scott,[d] Ø. Prytz,[c] A. E. Gunnæs[c] and G. Helgesen[bc]

Received 11th October 2013
Accepted 14th November 2013

DOI: 10.1039/c3nr05419e

www.rsc.org/nanoscale

The dielectric response of pentagonal defects in multilayer graphene nano-cones has been studied by electron energy loss spectroscopy and *ab initio* simulations. At the cone apex, a strong modification of the dielectric response is observed below the energy of the π plasmon resonance. This is attributed to $\pi \rightarrow \pi^*$ interband transitions induced by topology-specific resonant π bonding states as well as π^*–σ^* hybridization. It is concluded that pentagonal defects strongly affect the local electronic structure in such a way that multi-walled graphene nano-cones should show great promise as field emitters.

1 Introduction

The local electronic structure of carbon allotropes such as graphene[1–3] and carbon nanotubes (CNTs)[1,4,5] is strongly affected by topology. More specifically, these materials can exhibit an increase in the local density of states (LDOS) close to the Fermi level depending on the type, number and relative positions of topological defects.[2–5] Due to an apical localization of such states, graphene cones have been proposed as potentially excellent field emitters,[2,3] as have CNTs.[4,5] While this has yet to be confirmed experimentally for either single-layer graphene or graphene nano-cones,[6] cold field (CF) emission has recently been demonstrated in a working device for a cone-shaped carbon filament, which exhibits properties (such as brightness, current stability and spatial coherence) clearly exceeding those of traditional tungsten CF emitters.[7]

In the simplest case, a topological defect in graphene consists of a single pentagon or heptagon incorporated in the hexagonal lattice. More complex defects can be formed by combining pentagons and heptagons into defect pairs. One or more such pairs are found as the primary constituents of graphene grain boundaries[1] as well as in 'molecular junctions' that seamlessly connect CNTs of different helicity.[5] A direct consequence of incorporating pentagons in graphene is the reduction of the planar symmetry, resulting thus in positive curvature.[1] As a function of the number of pentagonal defects (P), this induced curvature leads to distinct three-dimensional nano-shapes such as cones (P = 1–5),[2,3,6] fullerenes (P = 12)[8] and caps (P = 6) at the ends of CNTs.[5] (By extension, the P = 0 case is often thought of as a cone without any curvature, *i.e.* a disc.) Fig. 1 illustrates the geometric 'construction' of a cone with one pentagon at its apex (Fig. 1(a)) by removing a 60° wedge from the honeycomb lattice (Fig. 1(b)) and 'sewing' the remaining edges back together (Fig. 1(a)). By repeating this process for each new pentagon a disclination of TD = $P \times 60°$ is formed.[6]

While CNTs[5] and fullerenes[8] have been extensively studied in the literature, conical carbon shapes have received significantly less exposure, possibly due to their relative rarity. In 1997, Krishnan *et al.*[6] were the first to observe graphene nano-cones with all five possible disclination angles. These cones are isolated, hollow and multi-walled carbon nanostructures, where the cone topology (P = 1–5) is given by the corresponding characteristic apex angle (112.9°, 84.2°, 60.0°, 38.9° and 19.2°). These discrete apex angles are predicted analytically by applying Euler's formula to the six-fold symmetry of graphene and the

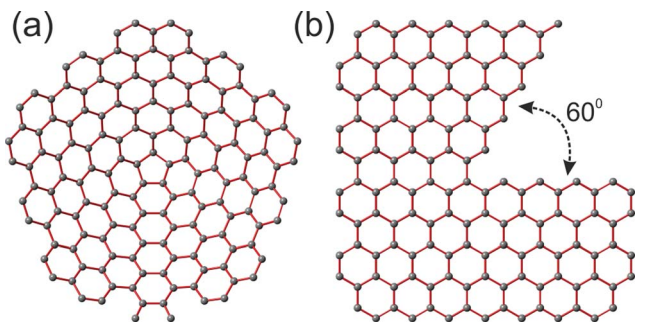

Fig. 1 Formation of a single pentagon graphene cone (a) by 'removing' a 60° wedge (b) from the graphene sheet and subsequently 'sewing' the remaining edges back together, creating a 60° disclination (a).

[a]*SuperSTEM Laboratory, SciTech Daresbury, Keckwick Lane, Daresbury, WA4 4AD, UK. E-mail: fshage@superstem.org; qmramasse@superstem.org; Fax: +44 (0)1925 86 4910; Tel: +44 (0)1925 864 903*

[b]*Physics Department, Institute for Energy Technology, P.O. Box 40, NO-2027, Kjeller, Norway*

[c]*Department of Physics, University of Oslo, P. O. Box 1048 Blindern, NO-0316, Oslo, Norway*

[d]*Institute for Materials Research, SPEME, University of Leeds, Leeds, LS2 9JT, UK*

cone geometry is therefore directly and exactly linked to the number of pentagonal defects present at their apex.[6]

Topology-induced changes in the electron structure of nanostructures can be observed indirectly by monitoring their response to an external electromagnetic field. This interaction is described by the complex dielectric function, $\varepsilon = \varepsilon_1 + i\varepsilon_2$, as a function of energy loss, E, and momentum transfer, $\hbar q$.[9] Local maxima of the imaginary component, ε_2, can be attributed to single electron interband transitions, while zero crossings of the real component, ε_1 (combined with a vanishing ε_2), correspond to plasmon excitations.[9] As the low loss part of an electron energy loss spectrum (EELS) is proportional to the loss function, $Im(-1/\varepsilon)$,[9] EELS in an aberration-corrected scanning transmission electron microscope (STEM) is the ideal tool for probing the dielectric response of nano-particles as it combines both high spatial and energy resolution.

In this paper we report observations of a topological modification of the electronic structure of multilayer graphene nanocones through STEM-EELS and *ab initio* simulations. This modification is consistent with an apical localization of low energy states,[2,3] which we suggest could make graphene nanocones highly promising field emitters.[2,3]

2 Experimental and computational section

2.1 STEM-EELS measurements and data analysis

The nano-cones studied in this work were produced by pyrolysis of crude oil with a plasma arc.[10] This pyrolysis procedure leads to the formation of a graphene cone kernel enveloped by a thick, less-ordered outer carbon layer. These 'coated' kernels are subsequently graphitized by heat treatment at 2700 °C for 11 h in an inert atmosphere to form the multilayer graphene structure.[11] Note that the cone structure distinguishes itself from that of graphite in the sense that instead of a strict AB Bernal stacking, the graphene layers comprising the cones lack any well-defined stacking order.

The resulting cones are hollow three-dimensional multilayer structures closely related to graphene, whose discrete range of apex angles dictates a direct correlation between the cone geometry and the number of topological pentagonal defects present at the apex of the successive layers, as described above.

All experimental measurements were carried out on a Nion UltraSTEM100 aberration-corrected dedicated scanning transmission electron microscope (STEM), equipped with a Gatan Enfina electron energy loss (EEL) spectrometer. The microscope was operated at an acceleration voltage of 60 kV to minimize irradiation damage[12] and retardation losses,[13] both known sources of spectral artifacts. It has recently been shown that under similar conditions (albeit on a wedge shaped Si <110> sample), it is possible to reliably observe energy loss features down to ~1.1 eV.[14] A convergence semi-angle of 30.6 mrad and a spectrometer collection semi-angle of 3.2 mrad were used, resulting in an electron probe size of 1.1 Å. Spectra were acquired with a dwell time of 0.15 s and a dispersion of 0.1 eV per channel at an energy resolution of 0.3–0.4 eV. The energy resolution was measured from the full width half-maximum of the 'zero loss peak' (ZLP).

The asymmetric ZLP profile significantly affects observed spectral intensities up to an energy loss of ~6 eV.[15] Thus, prior to Gaussian fitting, the ZLP contribution was estimated, and subsequently subtracted, by fitting of a power law to the low energy tail of the ZLP. The errors in peak positions shown are estimated from the statistical standard deviation from a significant number of measurements of the π and π + σ plasmon peaks at equivalent positions and acquisition conditions: 18 spectra were typically used here. Note that for sufficiently thin samples, a reduction in thickness is known to increase the probability of surface mode excitation, progressively '*red-shifting*' the observed value of the π and π + σ plasmon peaks.[9,15] The effect of this was deemed to be insignificant here as all spectra were obtained from homogeneous areas of constant and comparable thickness.

2.2 DFT simulations

Regarding the *ab initio* methodology, the CASTEP density functional theory (DFT) code[16,17] was used throughout all simulations. CASTEP is a pseudo-potential code that uses a plane-wave basis set to solve the Schrödinger equation. Loss and dielectric functions were modeled using the 'Optics' module of the CASTEP code, where the imaginary part of the dielectric function ε_2 is calculated within the random phase approximation (RPA)[9,18] for $(q \rightarrow 0)$ and the real part ε_1 is found through Kramers–Kronig relationships.[9] The loss function $Im(-1/\varepsilon)$ is then given by the resulting complex dielectric function $\varepsilon = \varepsilon_1 + i\varepsilon_2$. In order to reflect the energy resolution of the STEM-EELS spectra, all resulting loss and dielectric functions are broadened by a 0.3 eV Gaussian function. The authors note that for nanostructures this approach is not necessarily accurate in all cases as relativistic[19] and local field effects (LFEs)[20,21] are neglected here. Whilst acknowledging this and recognizing that further calculations might be needed for a fully quantitative comparison between simulations and experiments, the simulations presented here were found to be in good qualitative agreement with experimental results and highly useful in their interpretation.

In a DFT code such as CASTEP, the two key parameters are the kinetic energy cut-off and the density of *k*-points, which sample the reciprocal space in which the code operates. Convergence tests were carried out on the standard AB stacked graphite system,[18] using a generalized-gradient approximation (GGA) for the pseudo-potential and the Tkatchenko-Scheffler (TS) correction scheme to account for inter-plane Van der Waals interactions.[22] Parameter convergence was reached when the overall system energy varied by less than 0.005 eV, leading to a kinetic energy cut-off value of 660 eV and an average *k*-point separation corresponding to 0.03 $Å^{-1}$ or better in reciprocal space.

In terms of the structures that were built and simulated, geometry optimization has a subtle effect on the structure of bulk graphite, changing the lattice parameters to $a = b = 2.45$ Å

and $c = 6.68$ Å, whilst leaving the system symmetry unaltered. These parameters were used for the graphite results as presented. For ABA stacked trilayer graphene, layers were separated by a 3.4 Å interlayer spacing, as geometry optimization had almost no effect on the predicted spectra. In order to eliminate '*bleeding*' effects from neighboring '*cells*', a vacuum spacing of at least 30 Å in the '*c*' direction (*i.e.* perpendicular to the graphene planes) was used.

In the case of the cones, all modeled structures were based on previously reported apex angles[6] and pentagon arrangements.[2] For all three topologies, three 'layered' AAA stacked cones were modeled inside a 'cell' so that the structure was isolated in space by 20 Å or more in each dimension, with layers separated by 3.34 Å (the optimized layer separation for graphite). This size of vacuum was confirmed as sufficient by qualitatively comparing the polycrystalline loss function for model systems with different vacuum sizes. Fig. 2 shows top (a–c) and side views (d–f) of the modeled cone structures with one (a and d), two (b and e) and three (c and f) pentagons at the apex. When applying geometry optimization to the modeled cone structures, they tended to 'flatten' and exhibit apex angles well below that of the ideal structures.[6] This is probably due to the limited accuracy with which cone structures could be modeled as well as to the small sizes of studied systems. Thus, geometry optimization was not used in the final cone simulations.

The aforementioned convergence parameters were found to be adequate for modeling of the dielectric response in the CASTEP 'Optics' module. This was determined from progressive (and independently from each other) doubling of the kinetic energy cut-off and density of the *k*-point grid until no significant changes were introduced in the *polycrystalline* graphite loss function. The term polycrystalline, as used here, refers to an average over all possible directions of momentum transfer – akin to probing a sample containing a significant amount of randomly oriented crystallites. In post-processing, all loss and dielectric functions were polarized with momentum transfer along the crystallographic *a*/*b* and *c* axes (graphite and trilayer graphene), or along the *x*/*y* and *z* axes (cones). Here, in-plane loss functions of graphite and trilayer graphene were found to be identical, regardless of polarization along *a* or *b*. This is consistent with the reported electronic structure of graphite, where in-plane anisotropy vanishes at the Γ point (*i.e.* $q \rightarrow 0$) of the Brillouin zone.[18] A similar result was found for the one and three pentagon cones where loss functions were identical for polarization along the *x* and *y* directions. Thus, it is concluded that polarization along two perpendicular (in and out-of-plane) axes of anisotropy is sufficient for describing the dielectric response of the one and three pentagon cones as well as that of trilayer graphene and graphite. However, for the two pentagon cone subtle differences were found for polarization along the *x* and *y* axes. This effect was attributed to symmetry as can be seen from Fig. 2(b). To make for a suitable comparison to the results from other modeled structures, the in-plane dielectric response of the two pentagon cone is therefore given by averaging results polarized along the *x* and *y* directions, subsequently denoted by $q||xy$.

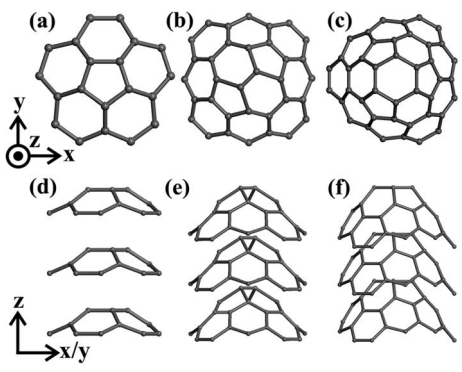

Fig. 2 Top (a–c) and side (d–f) views of the idealized cone tip structures whose optical properties were modeled by the CASTEP code. From left to right, cone apex angles are given by the number of pentagons (1–3).

3 Results and discussion

Fig. 3(a) shows a high angle annular dark field (HAADF) image of a multilayer graphene nano-cone with an apex angle of ~90°, which corresponds to a cone topology with two pentagons at the apex. The deviation from the theoretical 84.6° 'Euler angle'[6] can be attributed to a combination of measurement error, relative projection[11] as well as possible imperfections in the structure.[23] Fig. 3(c) and (d) show low loss EEL spectra obtained from the cone 'inner' apex at the position indicated in Fig. 3(b), plotted

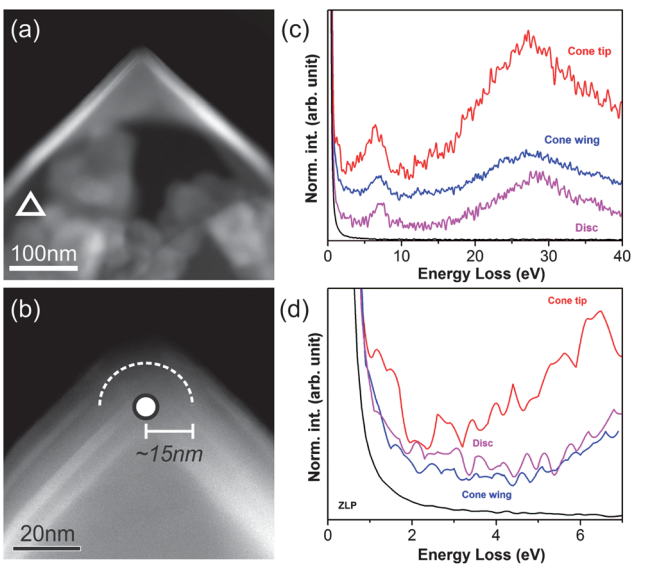

Fig. 3 STEM- HAADF images of (a) a carbon cone and (b) the cone tip. The measured ~90° apex angle corresponds to two pentagons at the tip. (c and d) Loss spectra from the cone apex (indicated by the white circle with black circumference in (b)), a cone 'wing', a disc and the vacuum ZLP averaged over 4 spectra. The ~1.5 eV cone tip loss feature in (d) is observed up to ~15 nm towards the edge of the cone, as indicated by the dashed semi-circle in (b). An example of the position of a cone 'wing' is indicated by the white triangle in (a).

for comparison against spectra from a cone 'wing' and a flat multilayer disc. This comparison is necessary to evaluate the effect of curvature as well as topology on the spectra. Here, a cone 'wing' refers to the open-ended side of a cone wall, an example of which is indicated in Fig. 3(a). In turn, multilayer discs can be regarded as cones with zero pentagons at their apex and are found in significant quantities in the pyrolytic powder sample.[6] Finally, in order to estimate the contribution of the zero loss peak (ZLP), a loss spectrum averaged from 4 acquisitions in vacuum, is plotted alongside the cone and disc spectra.

The spectra in Fig. 3(c) reveal that the π and π + σ plasmon peaks acquired at the cone tip are '*red-shifted*' compared to the expected graphite plasmon response with $q||a$.[21] More specifically and after careful fitting with Gaussian functions, the π and π + σ peak positions of the cone tip were determined to be 6.40 ± 0.05 eV and 27.36 ± 0.08 eV, respectively, compared to 7 eV and 28 eV for bulk graphite.[21] For the cone 'wing' (resp. for the multilayer disc), the π and π + σ peaks appear at 6.78 ± 0.05 eV and 27.53 ± 0.08 eV (resp. 7.14 ± 0.05 eV and 28.5 ± 0.08 eV). The observed '*red-shift*' of the π and π + σ plasmon peaks appears to increase as a function of local curvature (Fig. 3(c)), *i.e.* from a flat disc, to the slightly curved cone 'wing', to the highly curved cone tip. Thus, this '*red-shift* ' effect is likely due to an increased contribution of the $q||c$ component of the dielectric tensor, resulting from an effective change of the sample orientation, as has been suggested for multi-walled CNTs[8] and demonstrated for graphite.[21]

Apart from the energy shifts of the π and π + σ plasmons, the most striking feature of the cone tip spectrum is a distinct peak observed at ~1.5 eV (Fig. 3(d)). The precise position of this peak, at an energy loss of 1.52 ± 0.07 eV, was estimated by averaging Gaussian fits of a substantial number of spectra obtained from the cone tip area. This peak is only discernible up to ~15 nm away towards the edge from the cone tip, in all directions, as measured by moving the electron probe by increments of 1.7 nm from the position denoted in Fig. 3(b). Such a reasonably high degree of localization[9,15] could potentially arise from a poorer signal towards the outer layers of the structure, in combination with the presence of additional defects and amorphous carbon near the surface. Nevertheless, the appearance of this peak at the cone tip only, and the fact that no such feature was ever observed in any of the cone 'wings' or discs, strongly suggests an effect of topology. This feature was observed at the apices of cones of different apex angles. However, no clear correlation with apex angle in terms of the intensity or position of the peak could be derived from these experimental observations.

This intriguing experimental observation was rationalized using *ab initio* simulations, as described above. Note that in Fig. 3(c), the values and the shape of the π and π + σ peaks of the cone tip spectrum (as well as those of the cone wing and disc spectra) roughly coincide with the bulk dielectric response of graphite.[21] In related structures such as carbon nanotubes[15,24] and concentric carbon spheres[24] it has been shown that a significant contribution of surface effects are characterized by surface loss peaks at 13–15 eV and 17–19 eV accompanied by a significant reduction in the π + σ peak intensity. As this was not

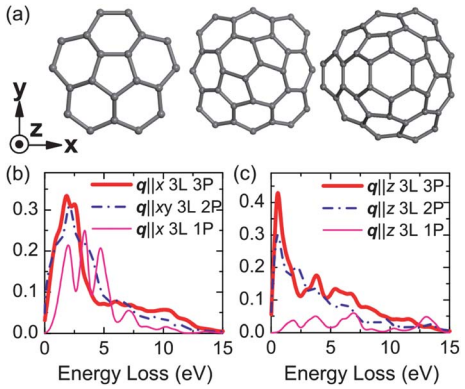

Fig. 4 (a) Top view of the modeled trilayer (3L) cone structures with one, two and three pentagons (1–3P) at the apex. Corresponding loss functions are polarized with momentum transfer along the (b) *x* (1,3 P) and (c) *z* axes. For the two pentagon cone (2P) the loss function in (b) is averaged along both the *x* and *y* directions.

observed in Fig. 3(c), it is assumed that surface effects are negligible in the probed volume. Thus the dielectric response can be understood in terms of the bulk dielectric function $Im(-1/\varepsilon)$, rather than a surface loss function.[9]

Trilayer AAA-stacked cone tip structures with up to three apex pentagons (Fig. 4(a)) were initially considered, where the calculated loss functions are polarized with $q||x$ or $q||xy$ (Fig. 4(b)) and $q||z$ (Fig. 4(c)), in analogy to $q||a$ and $q||c$ for graphite. The two and three pentagon loss functions exhibit similar shapes, both with maxima at 2.1 eV for $q||x$ or $q||xy$ and 0.6 eV for $q||z$. These loss functions are significantly '*red-shifted*' and 'sharpened' compared to the one pentagon loss function, for both polarization directions (Fig. 4(b) and (c)). Such a distinct difference can be explained by extended interactions between neighboring topological defects; this effect has been predicted when two or more pentagons are in close proximity at the cone apex.[2,3] To realistically simulate the loss spectrum, the fact that STEM-EELS measurements sample a finite region of momentum space must be considered. This means that recorded spectral intensities are given by an average over loss events occurring for momentum transfer both parallel and perpendicular to the direction of applied momentum transfer.[9] For the two pentagon cone for which experimental data are presented in Fig. 3, this means that any loss spectrum should include

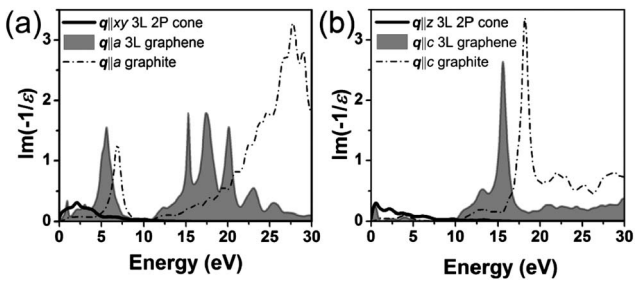

Fig. 5 (a and b) Modeled graphite, trilayer (3L) graphene and trilayer two pentagon (3L 2P) cone loss functions, polarized along their principal axes of anisotropy.

contributions from both $q||xy$ and $q||z$ components. Thus the maximum of the corresponding loss feature should appear at an energy between the $E(q||xy)_{max}$ = 2.1 eV (Fig. 4(b)) and $E(q||z)_{max}$ = 0.6 eV (Fig. 4(c)) peak values predicted by these calculations, which is in good qualitative agreement with the 1.5 eV feature observed experimentally (Fig. 3(d)). A similar peak is also predicted for three-pentagon cones (Fig. 4(b) and (c)).

While no π or π + σ plasmon peaks are predicted by our calculations for cones in Fig. 4, due in part to an effect of the size of the modeled structures and the fact that relativistic[19] and LFEs are being neglected,[20,21] the interpretation can be qualitatively extended to the entire energy range. Fig. 5 shows the calculated $Im(-1/\varepsilon)$ for AB stacked graphite and ABA stacked trilayer graphene with $q||a$ and $q||c$, in good agreement with the literature.[18,21,25] It has been suggested that long range geometry only plays a significant role below the π plasmon energy.[26] This is in perfect agreement with the experimental results, as the $q||a$ loss function of graphite (Fig. 5) only fails to qualitatively predict the cone tip spectrum at energies lower than that of the π plasmon resonance in Fig. 3(d). Thus the cone tip loss spectrum (Fig. 3(c) and (d)) can be represented by the calculated $Im(-1/\varepsilon)$ (Fig. 5) of graphite ($q||a$) for $E \geq E_\pi$ and cone ($q||xy$) for $E < E_\pi$. The predicted 6.9 eV, 27.7 eV ($q||a$) and 2.1 eV ($q||xy$) loss peaks appear again at slightly higher energies than those observed experimentally and, as previously discussed, the energy difference is likely due to the combined contribution of the $q||c$ and $q||z$ components and perhaps to the fact that LFEs are neglected.[20,21] Nevertheless, Marinopoulos *et al.*[27] showed for graphite, graphene and single-wall CNTs that while the introduction of LFEs results in significant corrections to the RPA out-of-plane dielectric response, any such corrections are comparatively small for the in-plane response, especially at energies below 10 eV. The loss spectra at the cone tip (Fig. 3(c) and (d)) are clearly dominated by an in-plane response rather similar to that of bulk graphite[21] (the convergent beam geometry, with a collection semi-angle of several mrad, playing an important role here). Furthermore, the ~1.5 eV peak is well below 10 eV. It is therefore expected that the incorporation of LFEs would not alter the presented RPA cone loss and dielectric functions to a large degree.

In order to evaluate the effect of the modeled structure thickness, the loss function of trilayer graphene is compared to that of the two pentagon cone (Fig. 5). Even though both structures are of equal thickness (*i.e.* three layers), the loss probability is significantly increased for the cone below the π peak energy. The agreement between the experimental and the modeled dielectric response for the cone is excellent however, and it is thus concluded that the increased intensity at the ~1.5 eV (Fig. 3(d)) loss peak is solely a result of local topology induced by the presence of pentagonal defects at the cone apex.

Indeed, a topologically induced ~1.5 eV loss feature reflects the predicted electronic structure of graphene cones, where localized states near the Fermi level result from the topological disorder created by pentagonal defects.[2,3] Fig. 6(a) and (d) show that ε_1 is far from crossing zero for the two pentagon cone: thus, no collective modes can be assigned below the graphitic π plasmon. We can therefore confidently attribute the ~1.5 eV peak to a sum over single electron transitions between topologically induced valence and conduction states. This agrees well with the literature where sub-π peak features in loss spectra from fullerenes[8] and CNTs[15,28] are attributed to π → π* interband transitions, and changes in this low energy dielectric response are assigned to a loss of degeneracy upon introducing more carbon atoms in C_{60} (ref. 8) and chirality in single wall CNTs.[28]

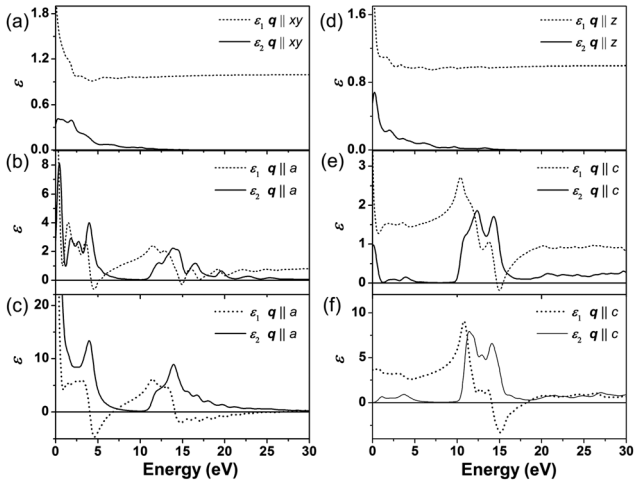

Fig. 6 Modelled real (ε_1:⋯) and imaginary(ε_2:—) components of the dielectric functions of (a and d) the two pentagon trilayer cone (2P 3L), (b and e) trilayer graphene and (c and f) graphite polarized along their principal axes of anisotropy as indicated in the upper right corner of each plot.

Some simple arguments can be put forward to explain why topological defects at the cone apices generate this sub-π energy feature. In pristine graphene, one π and three σ electrons are associated with each carbon atom. This changes upon the incorporation of a single pentagon, as the five carbon atoms show an 'affinity' for a sixth bonding π electron, resulting in an occupied resonant state screened by the other π electrons.[3] As previously mentioned, further interaction between resonant states is expected when two or more pentagons are in close proximity.[2,3] In the case of the cone apex, it is suggested that coupling between σ* and π* states significantly contributes to the local electron structure at the cone apex. Fig. 6(a) and (d) show that, for the two pentagon cone, ε_1 is larger than ε_2 in both directions of $\hbar q$, similar to the $q||c$ (Fig. 6(f)) rather than the $q||a$ (Fig. 6(c)) component of the graphite dielectric function. This indicates a significant 'σ character' as absorption peaks in the $q||$c graphite $Im(-1/\varepsilon)$ are attributed to symmetry-permitted π → σ* and σ → π* interband transitions.[18] The exact same trend can also be seen when comparing the dielectric function of the two pentagon cone (Fig. 6(a) and (d)) to the dielectric function of trilayer graphene (Fig. 6(b) and (e)), indicating that the thickness of these modeled structures does not play an important role here.

This increased 'σ character' might be related to curvature induced π*−σ* hybridization where π* and σ* states mix and repel each other, resulting in a red-shift of the π* and blue-shift of the σ* states compared to those of a planar geometry. Upon decreasing the radius of CNTs (*i.e.* increasing curvature) this

effect is expected to increase,[29] and as the local apical curvature is substantial in the cones, we argue that $\pi^*-\sigma^*$ hybridization is significant. This is consistent with a postulated[26] coupling between π and σ electrons upon reduction of the graphitic planar symmetry in carbon nanostructures. Following this argumentation, the $\sim$1.5 eV peak can be explained as a sum over $\pi \rightarrow \pi^*$ interband transitions determined by topology-induced resonant π states and $\pi^*-\sigma^*$ hybridization at the cone apex. It should be noted that these effects are highly sensitive to any deviation from the perfect conical structure: this was indeed observed for several cones for which the graphitization process resulted in a severe reduction in conical symmetry and in turn a suppression of the $\sim$1.5 eV peak. In addition, the observation of the $\sim$1.5 eV peak up to $\sim$15 nm from the apex 'center' (Fig. 3(b)) is attributed to the delocalized nature of the dielectric response[9,15] rather than the spatial extent of the states predicted to be highly localized for graphene cones.[2,3]

These findings have some important consequences for the application of multi-walled graphene nano-cones in field emission technology. The field emission properties of cone-shaped carbon structures (as opposed to the crystalline graphene nano-cones) are well-known: the conical shape of the carbon generates a high field enhancement factor at the tip, which reduces the applied voltage necessary for significant electron emission.[7] On geometrical grounds alone, the shape of the graphene nano-cones should thus ensure a similar effect, even without taking into account the apical topological defects. Importantly, states with a large LDOS close to the Fermi level are expected to supply the majority of emitted electrons, assuming they are localized in the high field region of the cone emitter. Here, the high field region corresponds to the region of maximal curvature, *i.e.* the cone apex.[2,3] The results and analysis presented above strongly suggest that these criteria are met for perfect multi-walled cones with a number of pentagons at the apex. The modification of the dielectric response of the cone due to the presence of these defects is in practice akin to an enhancement of the LDOS close to the Fermi level.[2,3] Hence, it is proposed that multilayer graphene nano-cones should show great promise for application as field emitters, as do CNTs.[5] But while for the latter the field emission properties are dependent on the diameter[5] and the relative position of pentagons near their closed extremities,[4,5] in the case of graphene nano-cones, the number of topological defects can easily be chosen by selecting those with the required characteristic apex angle.[6]

4 Conclusions

In conclusion, we show evidence for a distinct modification of the dielectric response by topological defects in graphene nano-cones. Specifically, the presence of two pentagons at the apex of a cone (which can be directly inferred from the cone geometry) results in a characteristic absorption feature in the low-loss spectrum below the energy of the π plasmon resonance. Attributed to a sum over $\pi \rightarrow \pi^*$ interband transitions, this peak is significantly '*red-shifted*' and increased in intensity compared to the planar graphite system. This is explained by interacting resonant bonding π states set up by the pentagonal defects as well as $\pi^*-\sigma^*$ hybridization induced by the high degree of curvature at the apex. Following this, we propose graphene nano-cones as promising field emitters, where the apical electronic structure can be controlled by selecting cones with a desired number of pentagons.

Acknowledgements

The authors gratefully acknowledge funding from the Research Council of Norway under grant number 191621/V30 and J.P. Pinheiro of n-Tec AS for providing cone samples. SuperSTEM is the UK Engineering and Physical Sciences Research Council (EPSRC) National Facility for aberration-corrected STEM. Computational work was undertaken using the ARC1 facility at The University of Leeds and CRS gratefully acknowledges the support of the high performance computing (HPC) team.

References

1 I. A. Ovid'ko, *Rev. Adv. Mater. Sci.*, 2012, **30**, 201–224.
2 C. Q. Qu, L. Qiao, C. Wang, S. Yu, W. T. Zheng and Q. Jiang, *IEEE Trans. Nanotechnol.*, 2009, **8**, 153–158.
3 J. C. Charlier and G. M. Rignanese, *Phys. Rev. Lett.*, 2001, **86**, 5970–5973.
4 D. L. Carroll, P. Redlich, P. M. Ajayan, J. C. Charlier, X. Blase, A. De Vita and R. Car, *Phys. Rev. Lett.*, 1997, **78**, 2811–2814.
5 J. C. Charlier, *Acc. Chem. Res.*, 2002, **35**, 1063–1069.
6 A. Krishnan, E. Dujardin, M. M. J. Treacy, J. Hugdahl, S. Lynum and T. W. Ebbesen, *Nature*, 1997, **388**, 451–454.
7 F. Houdellier, A. Masseboeuf, M. Monthioux and M. J. Hÿtch, *Carbon*, 2012, **50**, 2037–2044.
8 M. Terauchi and M. Tanaka, *J. Surf. Anal.*, 1997, **3**, 240–247.
9 R. F. Egerton, *Electron Energy-Loss Spectroscopy in the Electron Microscope*, Springer, US, 2011.
10 J. A. Bakken, R. Jensen, B. Monsen, O. Raanes and A. N. Wærnes, *Pure Appl. Chem.*, 1998, **70**, 1223–1228.
11 S. N. Naess, A. Elgsaeter, G. Helgesen and K. D. Knudsen, *Sci. Technol. Adv. Mater.*, 2009, **10**, 065002.
12 O. L. Krivanek, N. Dellby, M. F. Murfitt, M. F. Chisholm, T. J. Pennycook, K. Suenaga and V. Nicolosi, *Ultramicroscopy*, 2010, **110**, 935–945.
13 R. Erni and N. D. Browning, *Ultramicroscopy*, 2008, **108**, 84–99.
14 J. A. Aguiar, B. W. Reed, Q. M. Ramasse, R. Erni and N. D. Browning, *Ultramicroscopy*, 2013, **124**, 130–138.
15 B. W. Reed and M. Sarikaya, *Phys. Rev. B: Condens. Matter Mater. Phys.*, 2001, **64**, 195404.
16 S. J. Clark, M. D. Segall, C. J. Pickard, P. J. Hasnip, M. J. Probert, K. Refson and M. C. Payne, *Z. Kristallogr.*, 2005, **220**, 567–570.
17 M. C. Payne, M. P. Teter, D. C. Allan, T. A. Arias and J. D. Joannopoulos, *Rev. Mod. Phys.*, 1992, **64**, 1045–1097.
18 A. G. Marinopoulos, L. Reining, A. Rubio and V. Olevano, *Phys. Rev. B: Condens. Matter Mater. Phys.*, 2004, **69**, 245419.
19 M. Stöger-Pollach and P. Schattschneider, *Ultramicroscopy*, 2007, **107**, 1178–1185.
20 J. M. McMahon, S. K. Gray and G. C. Schatz, *Phys. Rev. Lett.*, 2009, **103**, 097403.

21 A. G. Marinopoulos, L. Reining, V. Olevano, A. Rubio, T. Pichler, X. Liu, M. Knupfer and J. Fink, *Phys. Rev. Lett.*, 2002, **89**, 076402.
22 A. Tkatchenko and M. Scheffler, *Phys. Rev. Lett.*, 2009, **102**, 073005.
23 F. S. Hage, The electronic structure and morphology of carbon fullerene nano-cones: an electron energy loss spectroscopy study, Ph.D. Dissertation, University of Oslo, ISSN 1501-7710, 2013.
24 M. Kociak, L. Henrard, O. Stéphan, K. Suenaga and C. Colliex, *Phys. Rev. B: Condens. Matter Mater. Phys.*, 2000, **61**, 13936–13944.
25 T. Eberlein, U. Bangert, R. R. Nair, R. Jones, M. Gass, A. L. Bleloch, K. S. Novoselov, A. Geim and P. R. Briddon, *Phys. Rev. B: Condens. Matter Mater. Phys.*, 2008, **77**, 233406.
26 A. Rivacoba and F. J. García de Abajo, *Phys. Rev. B: Condens. Matter Mater. Phys.*, 2003, **67**, 085414.
27 A. G. Marinopoulos, L. Wirtz, A. Marini, V. Olevano, A. Rubio and L. Reining, *Appl. Phys. A: Mater. Sci. Process.*, 2004, **78**, 1157–1167.
28 T. Pichler, M. Knupfer, M. S. Golden, J. Fink, A. Rinzler and R. E. Smalley, *Phys. Rev. Lett.*, 1998, **80**, 4729.
29 X. Blase, L. X. Benedict, E. L. Shirley and S. G. Louie, *Phys. Rev. Lett.*, 1994, **72**, 1878.